

Preliminary analysis of catenoid chimney cooling towers

Maciej WISNIEWSKI^{✉*}, Ryszard WALENTYŃSKI[✉], and Dawid CORNIK[✉]

Faculty of Civil Engineering, Department of Mechanics and Bridges, ul. Akademicka 5, 44-100 Gliwice, Poland

Abstract. Optimization plays an important role in scientific and engineering research. This paper presents the effects of using the catenoidal shape to design the structure of a chimney cooling tower. The paper compares some geometrical variations of the catenoid with the reference existing hyperboloidal structure. It also compares internal forces, deformation and stability of the catenoidal structure. The comparison shows some predominance of the catenoid over the popular hyperboloid structure of the shell. The paper attempts to find an optimal shape of the cooling tower in order to reduce the amount of material and labor. The paper utilizes engineering tools and the designing process for chimney cooling towers.

Key words: catenoid; shell; cooling tower; FEM; CFD.

1. INTRODUCTION

The following paper looks for the most efficient and cheapest theoretical shape in the construction of a natural draft chimney cooling tower. There already exist many works that concentrate on the construction and efficiency of chimney cooling towers. Examples include [1] and [2].

First known cooling towers dating from the end of the 19th century possess timber structures, a few meters in height. Applying concrete as the structural material allowed to build ~30m high cylindrical cooling towers. There was still a need to build more efficient i.e. taller towers, but cylindrical structures meet with the problem of stability. Next step in the evolution came with conical towers – Fig. 1, until Kuypers and Iterson proposed a hyperboloidal cooling tower in 1918 [3]. Timber or metallic natural draft cooling towers are still in use, however the largest plants use the hyperboloid ones.

The chief advantage of the hyperboloid structures is its negative Gaussian curvature, which provides good stability of the whole system. The hyperboloid is a ruled surface, so engineers were able to find internal-membrane forces using analytical methods. The shape of the hyperboloid and structural concrete have both been improved in the last 100 years, so modern cooling towers reach over 180 m in height. Because of their thin wall structure, hyperboloidal cooling towers also meet the problem of stability. Ruled surfaces contain straight lines, which may become a hot-spot of a buckling shape. Hence the idea of studying different shapes for chimney cooling towers has been deliberated.

Modern computational methods (i.e. FEM) allow one to find internal forces in the structure of any shape of the shell, not only

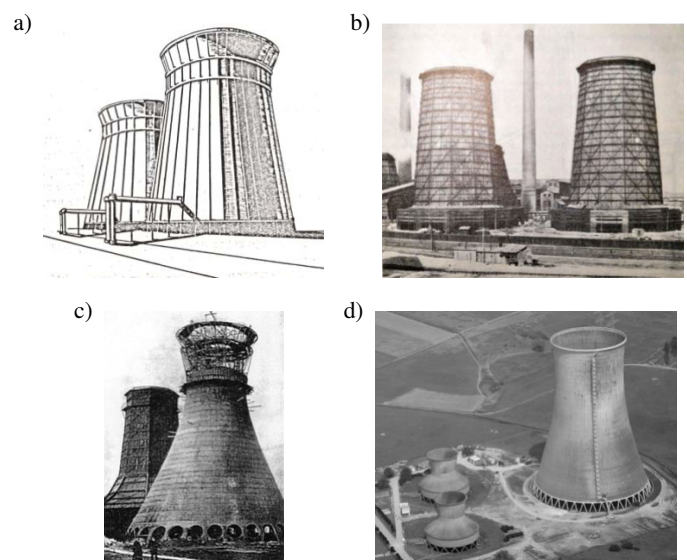


Fig. 1. Conical chimney cooling towers: a) concrete structure, b) timber structure, given by Ledwoń (1967) [2], c) first hyperboloid cooling tower, d) modern cooling tower [3]

the one given by a simple mathematical function. Some modern cooling towers are constructed by means of mixing a few different mathematical surfaces, like the combination of the hyperboloid (in the bottom) and a tube (in the upper part, above the thinnest cross-section). FEM allows us to analyze surfaces given by more complex equations, such as the catenoid, proposed 30 years ago [4]. Using computational methods, we are also able to determine the full set of internal forces, not only the axial forces in the membrane. There were also some attempts at optimization of shape, using FEM and Fortran scripting [5].

The analysis presented herein tries to use the catenoid as the geometrical representation of the chimney cooling tower shell provided as an alternative to the hyperboloid. The proposed so-

*e-mail: mwwisniowski@polsl.pl

Manuscript submitted 2023-04-23, revised 2023-08-05, initially accepted for publication 2023-09-01, published in December 2023.

lution offers hope for more efficient use of material and construction of a stronger structure.

2. METHODS

The study is based on scientific knowledge, norms and design codes, [6–10], as well as on engineering design practice. As a boundary condition for technological requirements, the environmental conditions and some structural solutions in the following study were applied to the technical data of the chimney cooling tower of the Opole Power Plant. The following paper does not optimize the whole structure, but looks for the parameter for the mathematical function that describes the shape of the shell. Parameters used in this paper as boundary conditions are as follows:

- height of the structure,
- bottom and minimal radiuses (throat height),
- shell thickness,
- material properties (normative parameters of specified concrete and steel).

These properties are constant throughout the study. The height of the thinnest section is the main variable in this study. For the reference structure in Opole, the value is equal to 122 m, and it was used as an initial parameter for the whole process.

The whole shell is a continuous surface that can be given by a mathematical function of the hyperboloid. The most important invention applied in this study is the change from the hyperboloid to catenoid function used, given by equation (1).

Modern authors [11] and also the newest standards recommend using FEM to find internal forces in the shell. For this reason, the RFEM 5.27 numerical software was used.

More attention is paid to wind load. Design codes do not precise the distribution of wind pressure for shapes such as the hyperboloid, catenoid or cone. They must be approximated by the cylindric shape. Using CFD allows us to analyze more accurate atypical shapes. Due to this reason, the wind load was considered in two different approaches. First, as recommended by the VGB standard and Eurocode procedure that are based on analytical and empirical equations. Second, by means of computational fluid dynamics (RWIND 1.27, which is based on OpenFoam). The results of the two approaches are compared in the next section.

2.1. Shape of the shell

The smooth shell of the cooling tower is obtained by revolution of the curve (1) around the vertical axis (z – in Fig. 2) in the middle of the coordinate system. A little transformation of the equation is made to insert the equation technical parameter of the structure inside. First, zero coordinates are placed at the bottom of the structure, so it is assumed that z' is equal to $z - h$. Parameters a and c are connected with the technical parameters of the structure (h, R_i), presented in Fig. 2. Parameters a and c are given by equation (2). When substituting them into equation (1), equation (3) is obtained and returns the coordinates of points that belong to the catenoid surface. The variable z varies from zero to H .

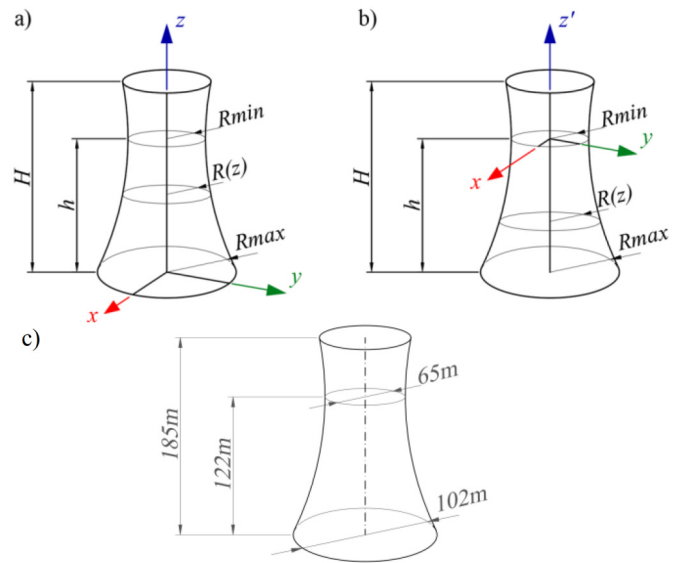


Fig. 2. a), b) Cooling tower shell. Coordinate systems, variables, and parameters, c) – dimension of reference model

Boundary condition of the study: the key radiuses, which do not vary throughout this study, are shown in Fig. 2c. Equation (4) defines the curve in the section of the hyperboloidal tower used in the paper as a reference model.

$$R(z') = a \cdot \cosh(z'/c) \quad (1)$$

$$\begin{cases} a = R_{\min} = 32.5 \text{ m}, \\ c = \text{arc cosh} [R_{\max}/R_{\min}], \end{cases} \quad (2)$$

$$R(z) = R_{\min} \cdot \cosh\left(\frac{z-h}{h} \cdot q\right),$$

where:

$$q = \text{arc cosh} [R_{\max}/R_{\min}], \quad (3)$$

$$R_{\text{hyp}}(z) = R_{\min} \sqrt{1 + \frac{(z-h)^2}{h^2} \cdot \left(\frac{R_{\max}^2}{R_{\min}^2} - 1\right)}. \quad (4)$$

The thickness of the shell is assumed as it was designed for the structure in the Opole Power Plant, and is equal to 20 cm along the entire shell, going up to 90 cm at the bottom.

2.2. Actions

The VGB standard points to the load actions that should be taken into account during static calculation. They are the following:

- self-load (gravity) (G)
- wind load (W)
- concrete contraction (shrink) (S)
- environmental temperature (T_{env})
- technological temperature (T_{tech})
- uneven ground settlements (B)
- dynamical response (D_{dyn})

The number of load combinations generated by Eurocodes is vast; however, the VGB standard [10] points to just two combinations that are reliable, i.e. equations (5) and (6). Limiting the number of combinations allows one to reduce the time required to analyze one case, and allows one to provide a more accurate calculation.

$$\begin{aligned} &\gamma_G \cdot G + 1.5 \cdot W + \gamma_Q \cdot B + \gamma_Q \cdot S, \\ &\gamma_G \cdot G + 0.9 \cdot W + \gamma_Q \cdot T + \gamma_Q \cdot B + \gamma_Q \cdot S. \end{aligned} \quad (5)$$

Monumental structures should be analyzed in consequence class CC3, so that each value of action is multiplied by factor 1.1, according to regulation [6]. The following analyses focus on gravity load and wind action. They are combined in one load combination:

$$1.485 \cdot G + 1.65 \cdot W. \quad (6)$$

Other load cases, as pointed out in this chapter, will be taken into account in future analysis. Gravity loads were considered based on geometry, density property and Earth acceleration, with a characteristic value of 25 kN/m³ with a value recommended by a Eurocode 2 [9] and literature [12, 13]. Due to the atypical shape, more attention was paid to the wind load.

2.3. Wind load

The wind load is applied as a pressure acting perpendicularly (and in some cases also tangentially) to the surface. Values can be obtained using the equations given by Eurocode 1–4 [8], as for the tube shape. A similar procedure for hyperboloids is provided by the VGB standard [10]. It is also easier in application than Eurocode, because it gives a full set of equations.

The distribution of wind pressure that varies with altitude above ground is given with precision by Eurocode [8]. It has been proven by many authors [2, 14, 15], and will not be discussed in this study.

In this study, the wind profile (Fig. 3a) is obtained, according to Eurocode, assuming:

- Basic wind velocity $v_{b,0} = 22$ m/s.
- Terrain category II – the most popular in flat regions where power plants are usually built.

There are many proposals in the literature on how to estimate wind load distribution in the radial direction, but most of them are limited to cylinder shapes. The analyses of the previous author showed that distribution of the wind pressure is quite different for the cylinder and catenoid (or hyperboloid). The hyperboloid cooling tower can be assumed to be a cylinder to determine the wind pressure; however, this simplification is not accurate enough for this analysis. Due to this reason, the following analysis uses computational fluid mechanics (CFD) to determine the distribution of wind pressure around the structure.

CFD estimation uses:

- k - ϵ turbulence model ,
- 2nd order, steady turbulent solver ,
- Wind enclosure size: 1000 m (wide); 500 m (high), 500 m (length before model), 1500 m (length behind model). Cross-section area $5 \cdot 10^5$ m², area of model projection $185 \cdot 9 = 1.76 \cdot 10^4$ m². (blockage ratio: 3.52%) .

- Surface roughness: $K_s = 0.0015$, roughness const. = 0.5.
- Turbulence intensity: 1% .
- Mesh size (global) 30 m; (near surface) 1.5 m.

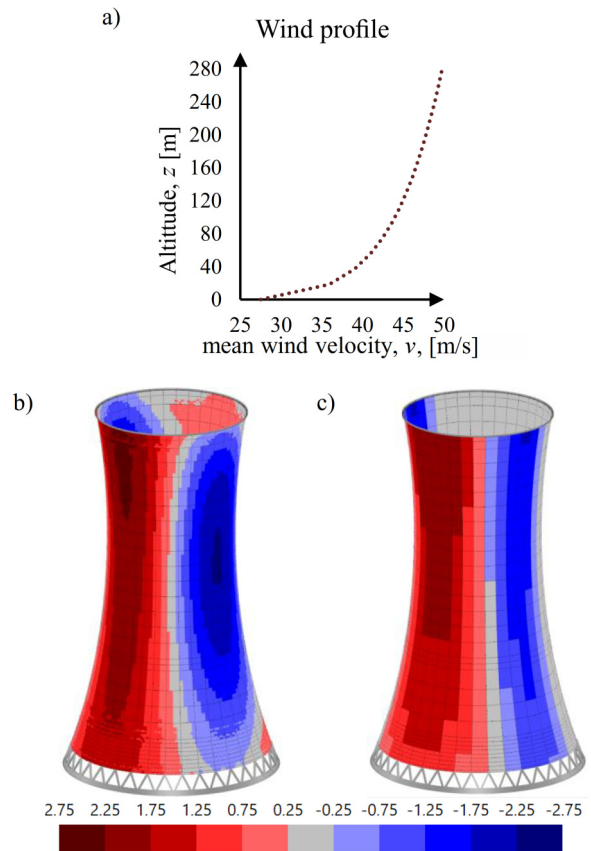


Fig. 3. a) Normative wind profile, b) Wind load on the chimney cooling tower obtained using CFD, c) wind load obtained using the equations given in the VGB standard [10], and by Eurocode [8] as for the cylinder. Presented in units [kPa] (pressure)

RWIND software has its limitations of application (in e.g. the quality of the boundary layer mesh, and steady flow only). Nevertheless analyses compare new-designed shapes, so using engineering software should be precise enough for this analysis.

The pressure distribution presented in Fig. 3, given by the equations (Eurocode) increases with the height above terrain, and the function of angular direction. The distribution obtained from numerical calculation seems to be more sensitive to local change of tower diameter. From the aerodynamic point of view, it can be explained, by the shape that accelerates the flow at the height of the smallest radius. There is a lack of scientific research in the field of aerodynamics around the hyperboloid. Nevertheless aerodynamics is not the subject of this paper. In further work, the authors will present more accurate experimental and numerical consideration.

2.4. FE model

Numerical calculations are performed in the RFEM Dlubal 5.27 finite element software. Numerical model of the shell uses surface elements (curved shells, divided into quadratic, 4-node

finite elements). The panels were modelled as homogeneous 'quadrangle' elements with linear stress distribution of constant thickness throughout its thickness.

The concrete shell is supported by 72 inclined members that represent the columns, and a horizontal member that represents the foundation beam. The boundary conditions were made with flexible support of the member. The analysis does not focus on uneven soil settlements, so the elastic model of soil seems to be precise enough. The member elastic foundation constant is equal to 60 MN/m² (vertically) and 6 MN/m² (horizontally). Figure 4. presents the orientation of the local axis for the foundation beams.

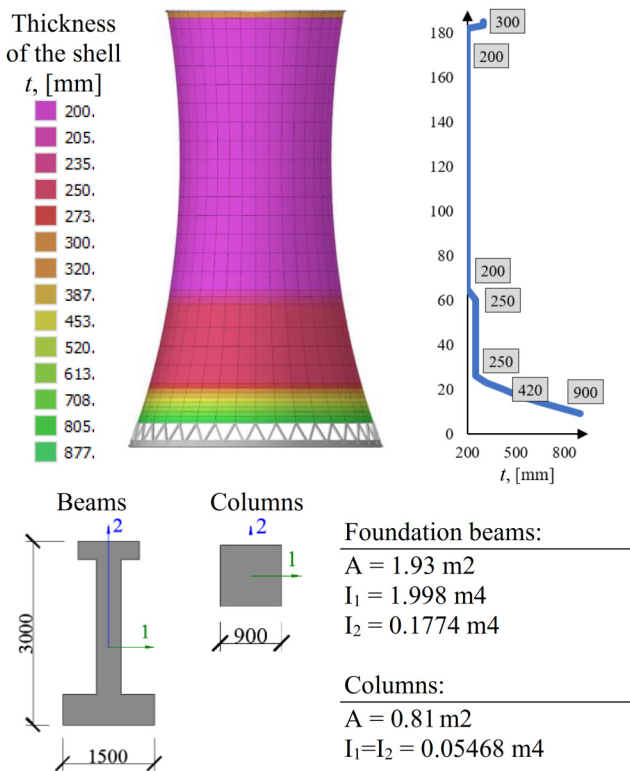


Fig. 4. Numerical model geometry – cross-sections and thickness

The quality of the finite element mesh has already been tested by Walentyński (2022) [16] and Rakowski (2005) [11]. The global mesh size divides the shell into 144 FE in the radial direction. In the bottom part of the shell, mesh refinement was applied using four times smaller elements. Figure 5 presents mesh refinements in the bottom of the shell. The finer mesh in the bottom area allows us to read more accurate results of the static calculation for local stresses and strains in the region between columns. However it makes no sense to use elements smaller than the column cross-sectional dimension above the columns. In that case, the whole force from the member element (column) would act on an area (size of 2 FE) smaller than the real size of contact between the column and the shell. It would produce enormous, false stress concentration and, in consequence, local plastic behavior and global deformation increase.

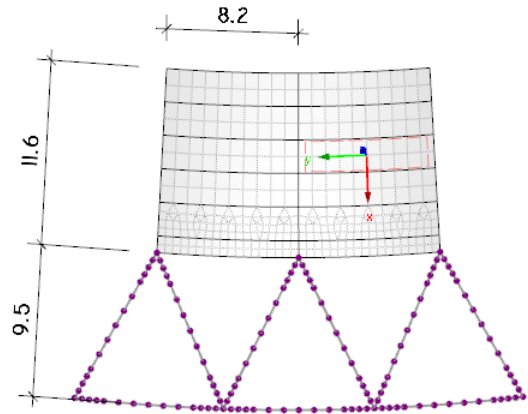


Fig. 5. Mesh refinement in the bottom. For clarity, only a section of the mesh is presented. Each of the 36 distances between the columns is divided into 18 finite elements. The global mesh set divides each 10° of the shell in the radial direction into 4 to 5 FE

2.5. Material and solver settings

Static calculation uses second order implicitly, i.e. large deformation solver (geometrically nonlinear analysis), which is suitable for large deformation of the system and thin wall structures. The solution is obtained by the Newton-Raphson method. Additionally, each load combination is divided in at least 10 load increments.

The Drucker-Prager material model is also considered for the homogeneous shell. The parameters of the material are set, as for concrete C35/45. The tensile yield limit of the material is obtained taking into account steel reinforcement (steel rod $\Phi 10$ each 10cm, booth direction and booth side). Assumed yielding stress and ultimate strength are a result of numerical analysis of the cross-section. Figure 6 shows the material parameters.

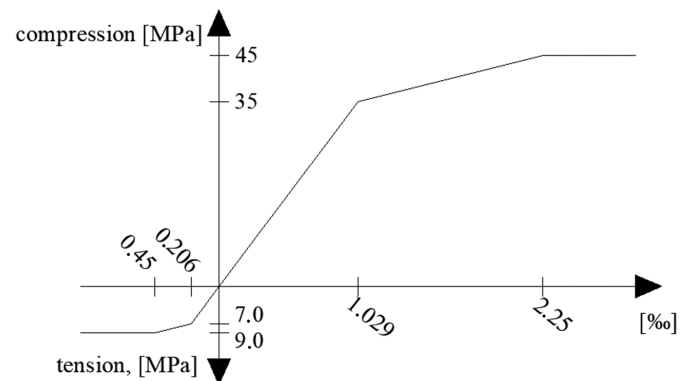


Fig. 6. Stress-strain graph assumed for homogeneous shell

3. RESULTS

Stress fields are the result of numerical calculations. Components of internal force, normal, shear forces and bending moments are products of stresses, obtained in post-processing of numerical calculation. This paper compares the internal structure of the shell for different geometries of the cooling tower. Because the thickness of the shell varies, the values for each

thickness should be compared separately. For this reason, the structure has been divided into 5 regions where the comparison is performed. Figure 7 shows the regions. In addition, the following are also compared: internal forces in 1d elements, axial for columns, and bending moments for foundation beams.

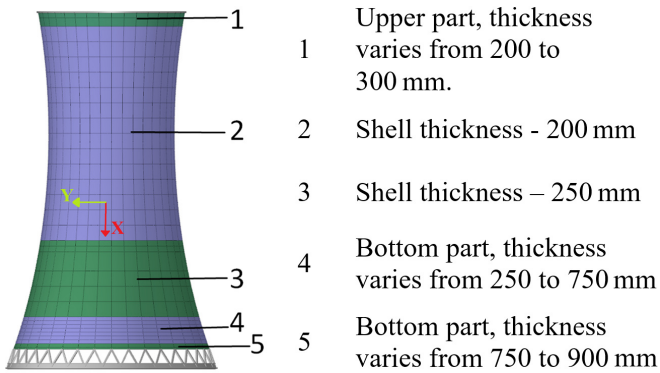


Fig. 7. Selected sectors of the shell to compare the results

Furthermore, internal forces are compared in 1d – member elements. The results discussed in this subsection refer to the catenoidal shell, with the parameter h fixed at 122 m, so the same as for the hyperboloidal reference structure.

It is important to note that during analysis plastic strain was not observed in most of the models. Limiting to elastic behavior is important for the durability and stiffness of concrete shell, which was described by Hojdy [13]. Large cracks accelerate carbonatization and significantly reduce the effective Young modulus of the shell.

3.1. Deformation

The major part of the deformation presented in Fig. 8 is the distortion component of the circular cross-section. Vertical displacements are of minor significance. The greatest deformation has a value of 231 mm, and it is observed at an altitude a little above the smallest cross-section. The ratio $\delta/D = 0.23/63 = 3.6\%$. There is less than acceptable geometric tolerance during

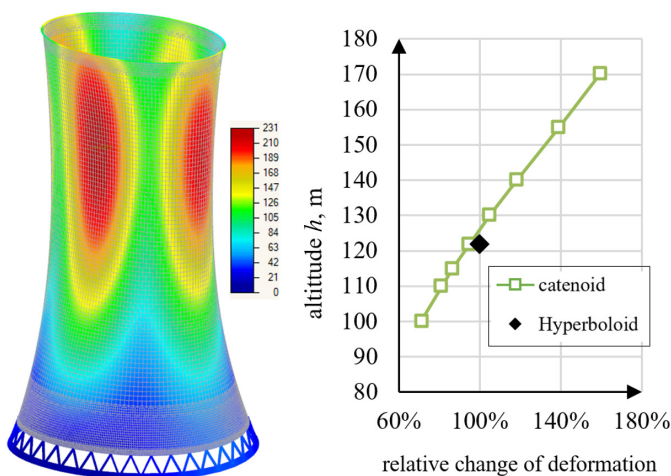


Fig. 8. Total deformation of the structure, and relative change with parameter h

construction. This shows that deformation with respect to the size of the structure is quite small. Because of this, the structure is considered rigid for the sake of CFD analysis, so one-way fluid-structure interaction is acceptable.

3.2. Shell behavior under applied load

For each region (Fig. 7), the extremal internal forces (n_x, n_y, m_x, m_y) have been compared on the graphs. Section 3.3 shows the comparison between the magnitude of the internal forces for each sample tested.

Figures in the next subsection show the distribution of internal forces for the catenoidal cooling tower, when the parameter h is equal to 122 m, so the same as for the reference hyperboloid structure. The local direction x refers to the meridional direction.

In the bottom and top regions, where thickness increases significantly, the internal forces also increase. To clarify the maps of forces, disturbed regions are hidden.

The shape of field stress (Figs. 9–12) is discussed in this subsection. For most of the shell (Fig. 9), there are compressive forces in the both – meridional and circumferential directions. Vertical forces reach values four times higher than the horizontal ones. Bending moments in the radial direction, which is responsible for distorting the circular cross-section, are visible throughout the whole height of the structure. Meridional bending appears mostly at the bottom of the structure (Fig. 10), where the thickness of the shell increases 4 times and is supported on the columns.

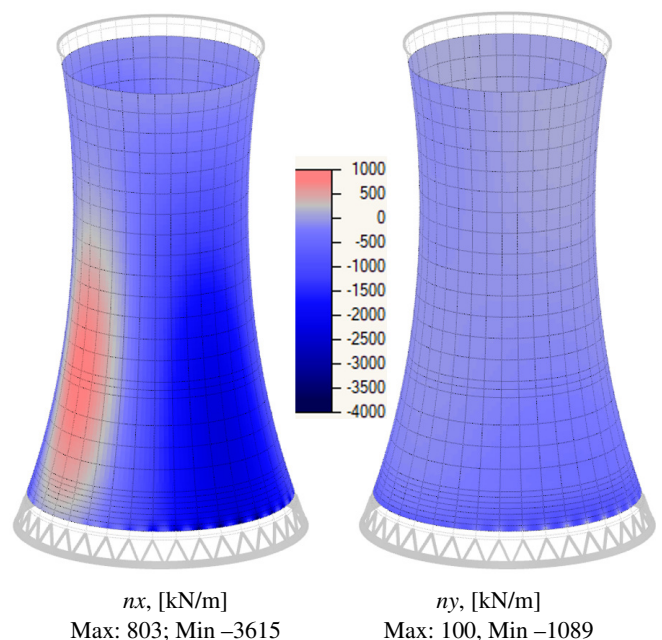


Fig. 9. Axial forces in the shell

Please note that the visible orthogonal mesh in all result pictures is not the FE mesh. Those are lines that belong to the surface. Lines are presented only for better visibility of curvature.

M. Wiśniowski, R. Walentyński, and D. Cornik

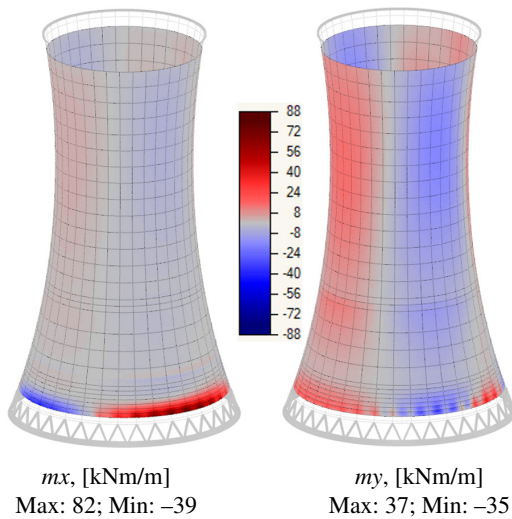


Fig. 10. Bending moments in the shell

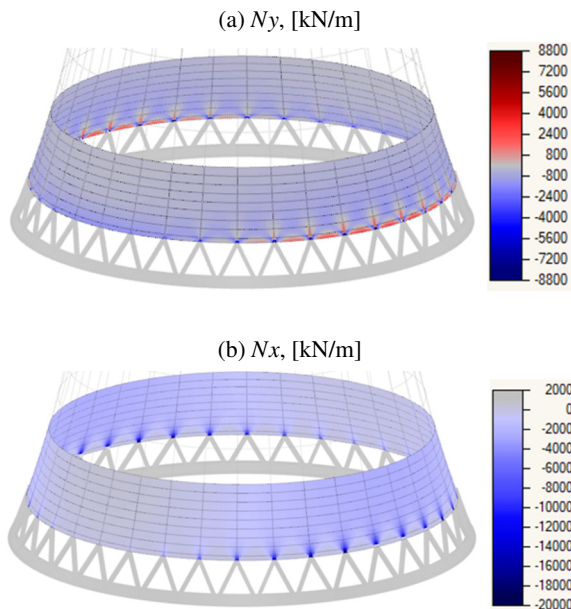


Fig. 11. Forces in the shell in the support region. (a) and (b) normal forces in orthogonal directions

The continuous distribution of internal forces in the lowest part of the shell is disturbed. In this region, there are some local bending effects and a concentration of stresses. Bending stiffness plays a more important role in that region. The local stress concentration above the columns (Fig. 11 and Fig. 12) requires additional check due to compressive and shear failure of the shell. The area of connection between the shell and the columns is not discussed here.

3.3. Change in internal forces in the shell

The relative change of each component of the set of internal forces is presented for each region separately in Fig. 13.

The graphs compare only the extremal value in the force field, so the values are not read from the same point of the shell.

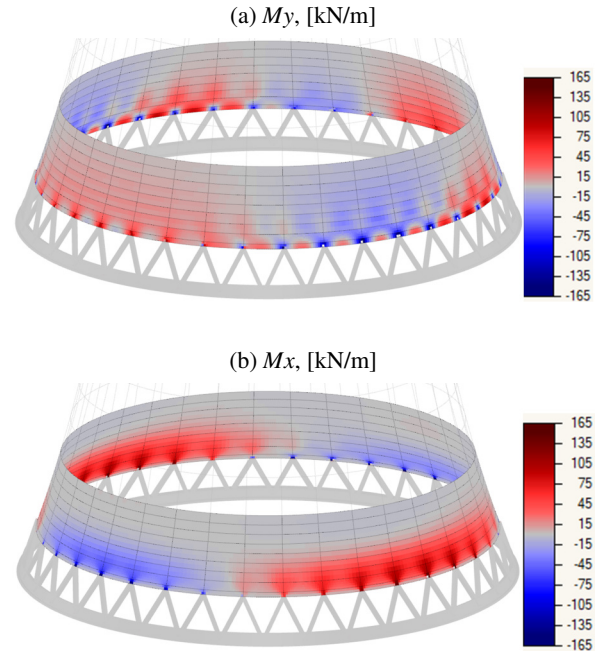


Fig. 12. Forces in the shell in the support region. (a) and (b) bending moments in the shell

The relative value of each model refers to the reference hyperboloid structure (existing structure in Opole Power Plant), with the relative base representing 100%. This was done to show better the change between the known solution and the proposed one. The vertical axis refers to the parameter h in equation (4).

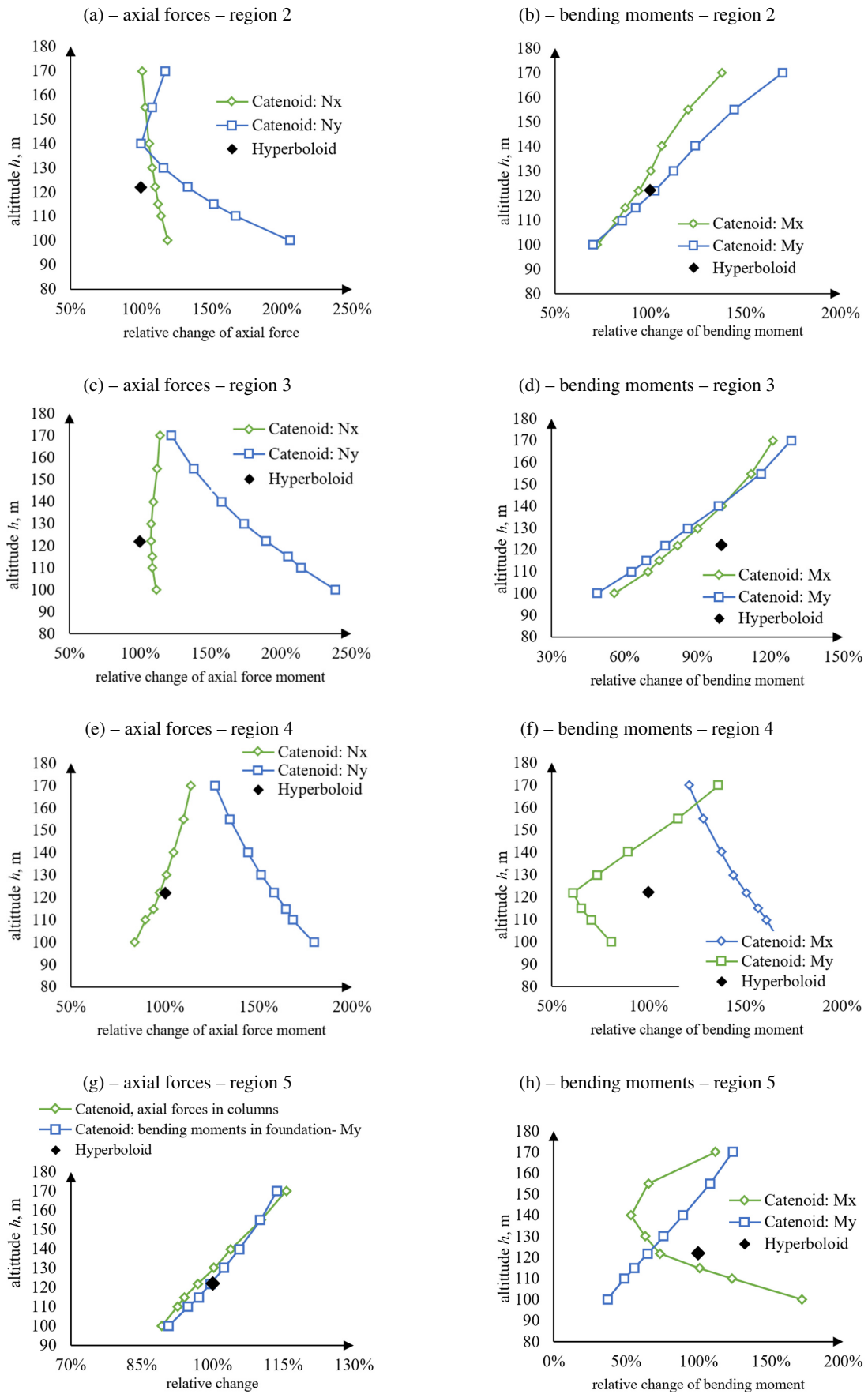
3.4. Stresses in the shell

The consideration of the previous author [16] showed that there is no common tendency in the graphs of internal forces. However, the forces are calculated on the basis of linear integration of stress, which is a real result of the numerical solution. Due to this, the stresses should also be taken into account in the comparison.

The principal stresses for the catenoid structure, with parameter h equal to 122 m, are discussed. Concrete structures handle compressive stresses well because the entire cross-section of the shell has some compressive strength. In case of tension, only steel bars take tensile forces in the calculation [17, 18]. Some old regulations allowed the consideration of the tension resistance of concrete [19], however, due to the more complex procedure, the tensile resistance of concrete is neglected in this analysis. Steel reinforcement is responsible for resisting all tensile stresses. The principal stresses measured at the surface are presented in the pictures below.

Figure 14 shows that the compressive stress throughout the shell reaches the value of 12 MPa. Tensile stresses reach a value of 4.6 MPa. The maximal values of stresses appear at the altitude where the shell changes thickness. Irregular distribution gives an effect of the asymmetric wind load acting on the surface. The highest values of stresses are observed in regions 2 and 3, where the thickness is equal to 200 and 250 mm, be-

Preliminary analysis of catenoid chimney cooling towers



cause the thickness of the shell increases in the bottom area, and the stresses decrease, except for the areas in the top of the columns.

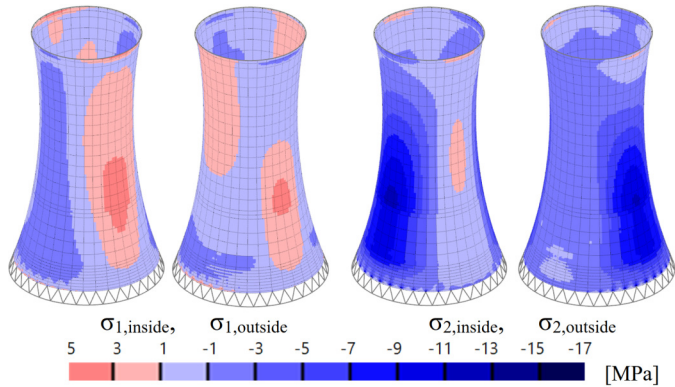


Fig. 14. Principal stresses on the side panels of the shell

From the point of view of stability, the stresses in sectors 2 and 3 are the most interesting ones. From an engineering point of view, it is easier to present stresses in the local orthogonal coordinate system, along the directions of the reinforcing bars in the shell. Figures 15 and 16 present the relative change in the stresses, given as a proportion of stress in the hyperboloidal reference structure.

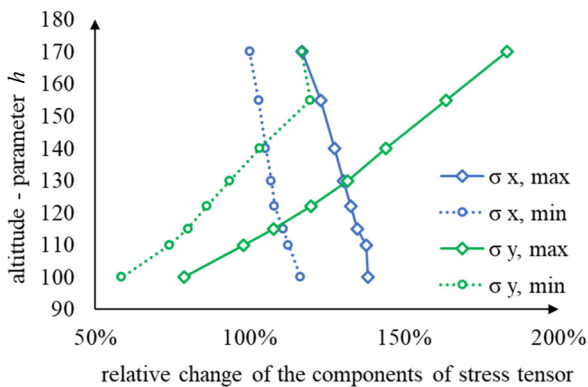


Fig. 15. Relative change of stress components with parameter h , for region 2 – shell thickness 200 mm

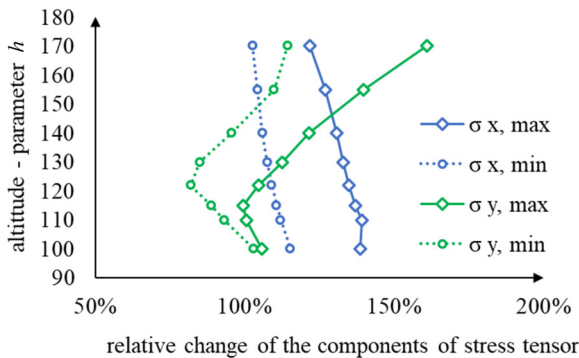


Fig. 16. Relative change of the stress components with parameter h , for region 3 – shell thickness 250 mm

The meridional stresses in the catenoidal shell decrease slightly with parameter h , when radial stresses increase significantly. The relative change of stress, for most tested catenoids, exceeds 100% and means that the components are smaller in the case of application of a hyperboloid. The best results for catenoids are obtained if the parameter h is between 120 and 140 m, with, in relation to the total height of the structure, $2/3$ to $3/4 H$. The total deformation of the shell increases with parameter h ; however, the relative increase is not significant.

3.5. Member elements and reactions

The relative change of forces in the member elements is also presented – axial forces in the columns and bending moments in the main axis of the foundation beam. The member elements are not the main subject of the study; however, they also play a role in total material use.

The variation of main internal forces given for the foundations and columns is shown in Fig. 17. The sum of vertical reactions and horizontal reactions in the direction of wind flow is presented in Fig. 18.

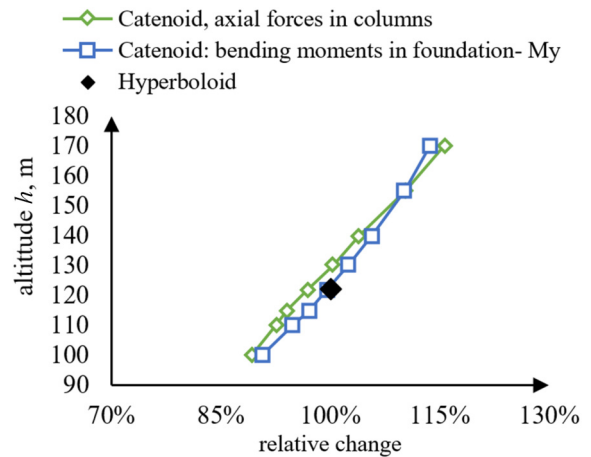


Fig. 17. Relative change of axial forces in the columns and bending moments in the beams

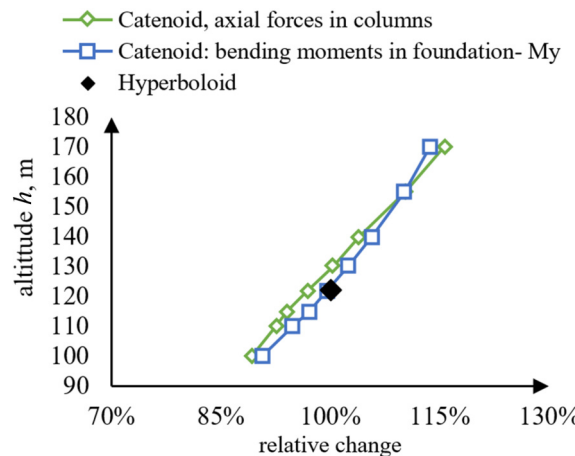


Fig. 18. Sum of reactions: Z – vertical; X – along the wind flow

3.6. Stability

The safety of thin-wall structures is also verified by checking the stability limit state [20]. The widely used method is the numerical approach, the critical load factor method. As a result of stability analysis, the critical load factor and the modal shape of the buckling are returned. For concrete elements, if the critical load factor is greater than 15, the influence of buckling can be neglected, and when the value is less than 1.0, this means that the structure is unstable under the load applied. For all tested chimney cooling towers, critical load factors are between 5 and 7, which means that the structures are rather safe; however, the influence of buckling effects should still be considered in the calculation.

The recommended method in this case is to apply geometrical imperfections as a pre-deformed mesh of finite elements. The shape of the deformation could be imported as a modal shape to compensate for lost stability or natural vibration. The best results of numerical calculation are always obtained when real shape of deformation is used, for example, result of 3D scanning. Unfortunately, the authors were unable to create 3D scanning even for existing structures. It should be mentioned that 3D scanning ($360 \times 360^\circ$), for example with the *Leica RTC360* device, takes approximately 30 s in the lowest resolution, when the period of natural vibration is equal to approximately 2 s. Therefore, the whole scan may include geometrical imperfections with a value of the vibration amplitude. Another method of considering imperfections is to increase the load by factor α :

$$\alpha = \frac{1}{1 - \frac{1}{f}} \quad (7)$$

Then second order moments are given by the following equation:

$$M_{II} = M_I \cdot \alpha \quad (8)$$

Using the second method and equations (7) and (8), the bending moment is approximately 3% lower for the catenoid than for the hyperboloid.

Figures 19a and 19b presents the first buckling shape. The comparison of absolute values of the critical load factor is presented in Fig. 19c.

The change in the critical load factor between the tested samples is small. Changes between 4.8 and 5.6 alter the second order moments in the elements by about 3%. For the samples tested, the meaning of stability analysis is small, but better stability behavior of the catenoid gives hope of building much higher cooling towers with the shape of the catenoid. The greatest results, therefore, of the stability factor, were obtained if the parameter h is equal to $3/4H$.

3.7. Dynamics of the shell

The last aspect of analysis is the dynamic behavior of the shell. Structures with circular cross-sections exposed to wind load, in some conditions, create a street shedding vortex [12, 14]. That transient and harmonic wind flow provides harmonic changes in wind pressure on the surface, which can be considered as a dynamic load. The most dangerous load case refers to the structure situated behind another circular structure that creates swirling flow. Next, in the case of a few chimney cooling structures located near each other, we can observe some transient wind flows. Many of those aspects of the wind were already well recognized [17, 21, 22]. Due to the dynamic character of the wind load, the design codes increase the pressure by a factor, depending on the natural vibration frequency. The factor increases the wind pressure given in the wind profile. The wind load applied in the following comparison also considers the factor.

Harmonic loads, with frequency close to the frequency of natural vibrations, can be especially dangerous due to the phenomenon of resonance [18, 23]. A study by the previous author [14] points out that:

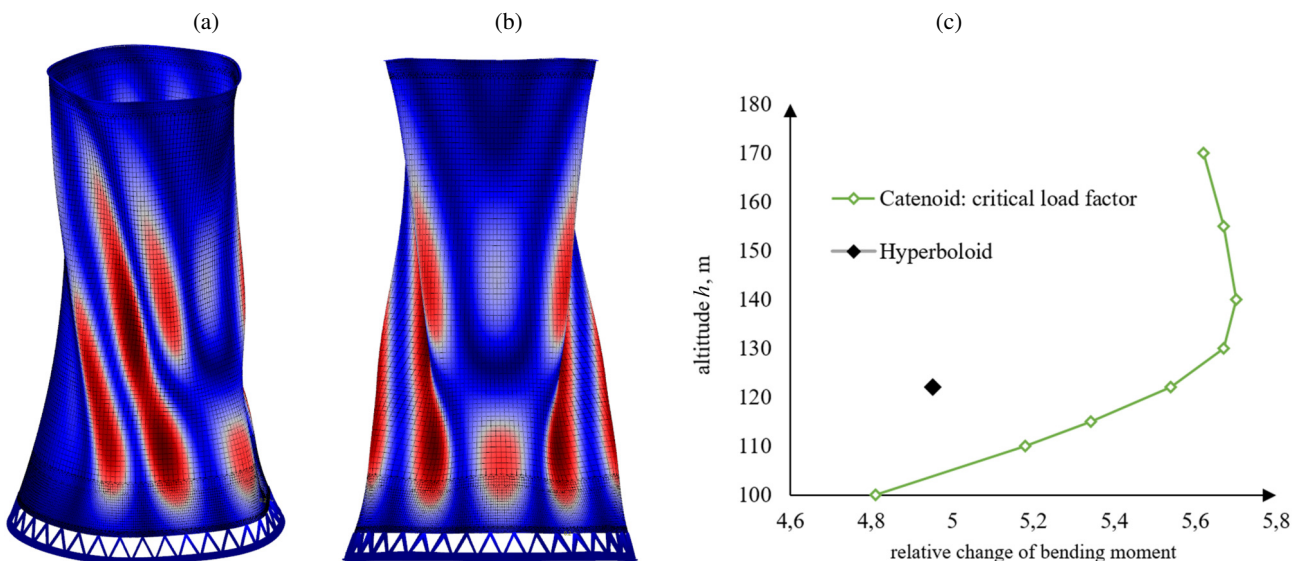


Fig. 19. Buckling analysis: deformation for the I-modal shape (a) isometric view, (b) front view (along wind direction), (c) relative change of critical load factor for tested samples

The potential vortex shedding for wind velocity of 40m/s and diameter of tower of 65 m will oscillate with frequency of approx. $f_o = 0.12$ Hz.

Based on work [23], Table 1 and Fig. 20 present frequencies of natural vibrations for tested structures. The natural frequencies are above 0.5 Hz, which is 4 times the vortex shading frequency. The structure should be safe; however, the influence of transient wind load should be considered (at least by the dynamic factor). The bigger the difference between the frequency of natural vibration and the changes in wind pressure, the better.

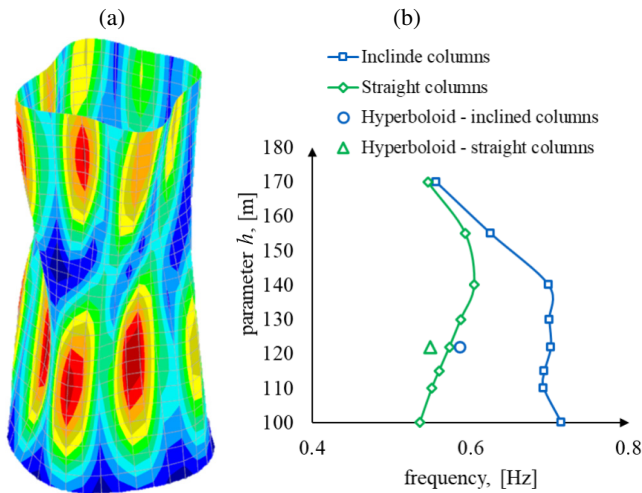


Fig. 20. a) First modal shape of natural vibration for the selected case, b) absolute change of frequency, 1st natural vibration mode with parameter h

Table 1

Natural vibration frequencies for chimney cooling towers

h	Frequency, f			
	Inclined columns		Straight columns	
	Catenoid	Hyperboloid	Catenoid	Hyperboloid
170	0.556		0.546	
155	0.625		0.593	
140	0.698		0.604	
130	0.699		0.587	
122	0.701	0.495	0.573	0.549
115	0.693		0.56	
110	0.692		0.551	
100	0.714		0.536	
[m]	[Hz]			

3.8. Validation of a numerical model

For the validation of numerical estimation of forces, a measurements in situ should be performed. The authors did not have financial possibilities to perform measurements on existing struc-

tures, so the validation is based on natural vibration measurements made by Shitang Ke in 2018 [13, 24].

Papers [13] and [24] present measurements of natural vibration frequencies on existing cooling towers in China. The model used in the following work was fitted (geometry and thickness of the shell) to the cooling towers named B and G in the work [24]. They are the Pingwei phase II project and the Shouguang Power station, respectively. The first natural vibration frequencies obtained from the FEM calculation and measured by Shitang are compared in the Table 2. Natural vibration shapes are presented in Fig. 21.

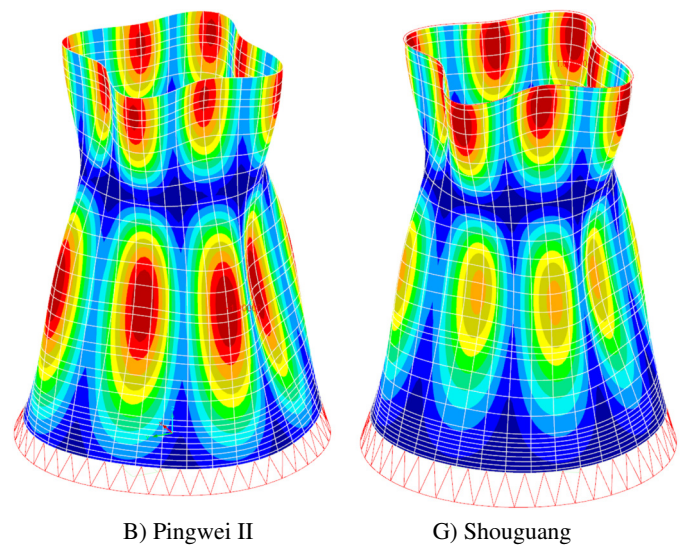


Fig. 21. First modal shape of natural vibration for validation models

Table 2

Validation of results

Tower	B) Pingwei	G) Shouguang
Total height	150	190
Height of throat	119	142.5
Radius (throat)	33	42
Radius (bottom)	57.4	141.6
Frequencies of 1st natural vibration mode [Hz]		
Authors FEM analysis	0.75	0.61
Measurement in situ	0.84	0.83
Relative error	11%	27%

High sensitivity of results, on some parameters, was observed during the validation. For example, equation (9) and Fig. 22 present sensitivity of results on the assumed boundary – the spring constant of Winkler support. The frequency of the results varies proportionally to the logarithm of the spring constant.

$$f \sim \text{Log}[C_{i,j}] \quad (9)$$

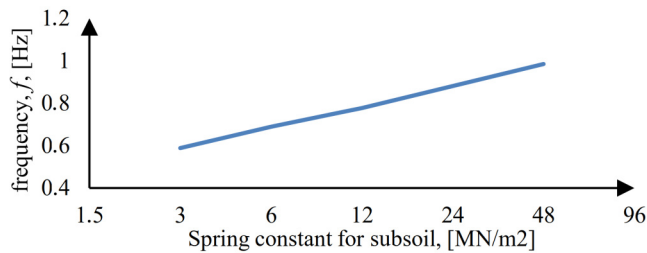


Fig. 22. Change in resulting frequency with subsoil constant parameter $C_{i,j}$

Unfortunately, most authors of measurements deliver only geometric data of structures, so knowledge about testing structures is incomplete. Nevertheless, it was possible to obtain similar frequencies of natural vibration.

Increase of mesh density 2.5 times causes a 0.2% change in result frequency, and for a 5-time increase the change is 0.4%, so the assumed mesh almost does not impact the result.

The sensitivity of the results to the assumed parameters shows that the values presented in this paper should be considered as comparison, not as guideline – at least as long as the whole boundary condition is not recognized well.

4. CONCLUSIONS

The study entailed structural static analysis of a hyperboloid and some variations of the catenoid shell. All geometries look quite similar, however, the assumed geometry may impact the results obtained or the total wind force acting throughout the structure. The sensitivity of the solution to the assumed boundary is quite concerning. The method used to determine the wind load significantly impacts the results. Unfortunately, the wind load is one of the most unpredictable loads, also difficult to simulate. Therefore, additional analysis, including wind tunnel testing, must be performed to establish the true stress fields. The authors are actually working on small-scale experimental research and an advanced CFD case study of wind flow around a cooling tower. There is also a lack of scientific research of aerodynamic amplification of wind speed near the structure by cooling towers. Other environmental and technological loads are supposed to be considered to be able to decide which cooling tower shape is the best.

During the analysis performed, some differences were observed; however, the catenoidal and hyperboloidal structures behaved similarly. A catenoid seems to face the stability limit state better, so it gives hope to be helpful in creating taller structures. Taking into account all the results presented, the best results can be obtained for the catenoidal chimney cooling tower if the thinnest cross-section is located at an altitude equal to $2/3 \div 3/4$ of total height.

It is also worth remembering that thin wall structures are very sensitive to boundary conditions. The design of monumental cooling towers, with very thin walls, requires a very well-recognized environment. Destructive tests for material samples and measurements of natural vibrations after erection are good verification of the validity of assumed parameters.

ACKNOWLEDGEMENTS

Publication supported as part of the Excellence Initiative – Research University program carried out at the Silesian University of Technology.

REFERENCES

- [1] G.B. Hill, E.J. Pring, and P.D. Osborn, *Cooling Towers. Principles and Practice*, London, Boston, Singapore, Sydney, Toronto, Wellington, Butterworth-Heinemann, 1990.
- [2] J. Ledwoń and M. Golczyk, *Chłodnie Kominowe i Wentylatorowe*, Warsaw, Arkady, 1967. (in Polish)
- [3] F. Afshari and H. Dehghanpour, “A Review Study On Cooling Towers; Types, Performance and Application,” *ALKÜ Fen Bilimleri Dergisi*, pp. 1–10, Mar. 2019
- [4] S. Bielak and R. Walentyński, “Powłoka katenoidalna – opis geometryczny, rozwiązanie ogólne umownego stanu błonowego i przykład dla osiowo-symetrycznego obciążenia ciężarem własnym,” *Zesz. Nauk. WSI*, vol. 36, pp. 39–52, 1993. (in Polish)
- [5] C. Kostem, “The determination of the shape and thickness of a thin minimum weight shell,” Ph.D. dissertation, University of Arizona, 1966.
- [6] *Eurocode Basis of Structural Design*, EN-1990, CEN, 2002.
- [7] *Eurocode 1: Actions on structures – Part 1-1: General actions – Densities, self-weight, imposed loads for buildings*, EN-1991-1-1, CEN, 2002.
- [8] *Eurocode 1: Actions on structures – Part 1-4: General actions – Wind actions*, EN-1991-1-4, CEN, 2005.
- [9] *Eurocode 2: Design of concrete structures – Part 1-1: General rules and rules for buildings*, EN-1992-1-1, CEN, 2004.
- [10] *Structural Design of Cooling Towers*, VGB-S610-00-2019-10-EN, VGB, 2019.
- [11] G. Rakowski and Z. Kacprzyk, *Metoda Elementów Skończonych w mechanice konstrukcji*, Warsaw, Oficyna Wydawnicza Politechniki Warszawskiej, 2005. (in Polish)
- [12] von T. Kármán, *Aerodynamics – Selected Topics in the Light of Their Historical Development*, Dover Publications, 1957.
- [13] S. Ke *et al.*, “Sensitivity analysis and estimation method of natural frequency for large cooling tower based on field measurement,” *Thin-Walled Struct.*, vol. 127, pp. 809–821, 2018, doi: 10.1016/j.tws.2018.03.012.
- [14] A. Flaga, *Inżynieria Wiatrowa. Podstawy i Zastosowania*, Warsaw, Arkady, 2008
- [15] A. Padewska, “Determination of the interference coefficients of cylinders in rows arrangement,” in *Współczesny stan wiedzy w inżynierii lądowej*, vol. 1, I. Pokorska-Silvan Ed., Gliwice, 2015. (in Polish)
- [16] R. Walentyński, M. Wiśniowski, and D. Cornik, “Catenoid cooling tower – introductory structural analysis” in *Lightweight Structures in Civil Engineering*, 2022, pp. 129–140.
- [17] G. Pankanin, “Numerical Analysis of Flow Averaging Tubes in The Vortex-Shedding Regime,” *Metrol. Meas. Syst.*, vol. 18, pp. 361–370, 2011.
- [18] D. Cornik, “Porównanie charakterystyk dynamicznych chłodni kominowych hiperboloidalnej i katenoidalnej,” M.S. thesis, Silesian University of Technology, Gliwice, 2020. (in Polish)
- [19] *Concrete, reinforced concrete and prestressed concrete. Design rules*, PN-84/B-03264, PKN, 1984.
- [20] M. Huihan, L. Zongyu, L. Shaozhen, S. Bingbing, and F. Feng, “Stability analysis and performance comparison of large-scale hyperbolic steel cooling towers with different latticed shell sys-

M. Wiśniowski, R. Walentyński, and D. Cornik

- tems,” *J. Constr. Steel Res.*, vol. 160, pp. 559–578, 2018, doi: [10.1016/j.jcsr.2019.05.042](https://doi.org/10.1016/j.jcsr.2019.05.042).
- [21] A. Flaga, R. Kłaput, Ł. Flaga, and P. Krajewski, “Wind tunnel model tests of wind action on the chimney with grid-type curtain structure,” *Archives of Civil Engineering*, vol. 67, pp. 177–196, 2021, doi: [10.24425/ace.2021.138050](https://doi.org/10.24425/ace.2021.138050).
- [22] M. Kabaciński, C. Lachowicz, and J. Pospolita, “Numerical Analysis of Flow Averaging Tubes in The Vortex-Shedding Regime,” *Arch. Mech. Eng.*, vol. 60, pp. 283297, 2013, doi: [10.2478/meceng-2013-0018](https://doi.org/10.2478/meceng-2013-0018).
- [23] K. Gromysz, *Dynamika Budowli. Obliczanie układów prętowych o masach skupionych*, Warsaw, PWN, 2017. (in Polish)
- [24] S. Ke *et al.*, “Full-scale measurements and damping ratio properties of cooling towers with typical heights and configurations,” *Thin-Walled Struct.*, vol. 124, pp. 437–448, 2018, doi: [10.1016/j.tws.2017.12.024](https://doi.org/10.1016/j.tws.2017.12.024).